ChemistryOpen

Full Papers
doi.org/10.1002/open.202000315

**Chemistry
Europe**
European Chemical
Societies Publishing

Pyridine-based Liquid-Phase Synthesis of Crystalline TiN and ZnSiN₂ Nanoparticles

Alexander Egeberg,[a] Olivia Wenzel,[b] Radian Popescu,[b] Dagmar Gerthsen,*[b] and Claus Feldmann*[a]

TiN and ZnSiN₂ nanoparticles are obtained via a novel pyridine-based synthesis route. This one-pot liquid-phase route strictly avoids all oxygen sources (including starting materials, surface functionalization, solvents), which is highly relevant in regard of the material purity and material properties. Colloidally stable suspensions of crystalline, small-sized TiN (5.4 ± 0.4 nm) and ZnSiN₂ (5.2 ± 1.1 nm) are instantaneously available from the liquid phase. Elemental analysis and electron energy loss spectroscopy confirm the purity of the compounds and specifically the absence of oxygen. The as-prepared ZnSiN₂ show yellowish emission (500-700 nm) already at room temperature with its maximum at 570 nm.

1. Introduction

Metal nitrides are most often prepared either by nitridation, i.e. redox reaction of a zero-valent metal with nitrogen, or by ammonolysis, i.e. acid-base reaction of a metal compound (most often metal oxides) with ammonia.[1] These approaches are hampered in the first case by the inertness of N_2 and in the second case by the difficulty to completely deprotonate the already basic NH_3. High temperatures (600–1500 °C) are usually required to perform the reactions, and impurities due to residual metal or metal oxides often cannot be avoided.

Aiming at metal nitride nanomaterials is even more challenging in comparison to bulk compounds, since the high temperatures needed for nitridation and ammonolysis are counterproductive to the formation of uniform, non-agglomerated nanoparticles.[1] Here, alternative synthesis strategies need to be explored and, for instance, comprise the thermal decomposition of nitrogen-rich precursors (e.g., silazanes, azides)[1,2] or ammonothermal reactions in supercritical NH_3 at high temperature and high pressure (up to 600 °C and 500 MPa).[3] Beside the realization of high-quality nanoparticles with narrow size distribution and low agglomeration, purity and crystallinity are additional challenges when aiming at metal nitride nanoparticles. Oxide impurities, which can be often not avoided when using oxygen-containing starting materials (e.g., metal hydroxides, metal nitrates, urea) can significantly deteriorate the material properties of metal nitrides even on a level of some hundred ppm.[4] To develop the full potential in regard of their material properties, moreover, the metal nitrides need to be crystalline, which results in conflicting requirements for synthesis. Thus, high temperatures are needed to promote the crystallinity, whereas low temperatures are required to guarantee a good size control and a low level of agglomeration.[5]

On the search of new liquid-phase synthesis strategies, we could recently show that nanoparticles of zero-valent metals (e.g., Fe(0), Mn(0), V(0))[6] as well as transition metal nitrides (e.g., Ni_3N, Cu_3N) can be realized via a liquid-phase synthesis using pyridine.[7] Based on the promising results, we here present the pyridine-based one-pot synthesis of TiN and ZnSiN₂ nanoparticles. Both are highly interesting in regard of their semiconductor-type properties, specifically including optical and catalytic features.[8] They also stand exemplarily for group 4 and group 14 metal nitride semiconductors.

2. Results and Discussion

2.1. Pyridine-Based Synthesis

TiN and ZnSiN₂ were exemplarily selected to explore the potential of the pyridine-based synthesis, since both compounds are interesting in regard of their material properties and since their synthesis as high-purity, high-quality nanoparticles is not possible so far. TiN nanoparticles were reported to be used for photocatalytic water splitting and electrocatalysis,[8c,9] as anode materials in high-power batteries,[10] or as plasmonic absorber.[8a,b,11] ZnSiN₂ is a highly promising semiconductor material for LEDs and specifically to replace the highly expensive GaN.[8d,e] In regard of the synthesis of nanoparticles, TiN was yet predominately prepared by ammonolysis of suitable precursors (e.g., TiO_2, $TiCl_4$, $Ti(NMe_2)_2$) at high temperatures ($\geq$ 500 °C),[12] by reaction of azides with Ti-alkoxides or $TiCl_4$,[13] or via gas-phase methods (e.g., laser

[a] Dr. A. Egeberg, Prof. Dr. C. Feldmann
Institut für Anorganische Chemie
Karlsruhe Institute of Technology (KIT)
Engesserstrasse 15, 76131 Karlsruhe (Germany)
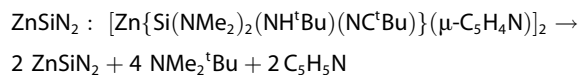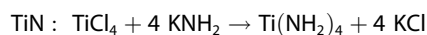E-mail: claus.feldmann@kit.edu

[b] Dr. O. Wenzel, Dr. R. Popescu, Prof. Dr. D. Gerthsen
Laboratorium für Elektronenmikroskopie
Karlsruhe Institute of Technology (KIT)
Engesserstrasse 7, 76131 Karlsruhe (Germany)
E-mail: dagmar.gerthsen@kit.edu

ChemistryOpen

Full Papers
doi.org/10.1002/open.202000315

Chemistry Europe
European Chemical
Societies Publishing

ablation, plasma deposition).[14] $ZnSiN_2$ was yet only prepared as microcrystalline powder and bulk sample, typically using high-pressure methods and/or ammonothermal synthesis.[15]

Based on this situation, TiN and $ZnSiN_2$ are interesting candidates to probe the potential of the pyridine-based synthesis route. Accordingly, $TiCl_4$ and KNH_2 as base were dissolved in pyridine to form a suspension of $TiCl_4(Py)_2$ and thereafter heated in an autoclave for 6 h at 300 °C. The formation of TiN can be directly visualized by the color change from a colorless $TiCl_4(Py)_2$ suspension to a deep black TiN suspension (Figure 1a). A similar reaction of $ZnCl_2$, $SiCl_4$ and KNH_2 was not successful and only resulted in amorphous Si–N–H species that turned to Si_3N_4 after sintering at 600–800 °C. This can be ascribed to the different acidity of $ZnCl_2$ and $SiCl_4$ as well as to the different solubility and stability of the zinc amide and silicon amide intermediates. As an alternative, we have selected the molecular single-source precursor $[Zn\{Si(NMe_2)_2(NHCMe_3)(NCMe_3)\}(\mu\text{-}NC_5H_4)]_2$, which was prepared following a recipe given by Jansen *et al.* (*SI: Figures S1,S2*).[15d] Thus, the single-source precursor was heated in an autoclave for 1 h at 280 °C and resulted in a colorless suspension of $ZnSiN_2$ nanoparticles (Figure 1b). Here, it needs to be noticed that low quantities of elemental zinc were observed in some samples,[15d] which precipitates in the form of large particles (>100 nm). In sum, the synthesis of TiN and $ZnSiN_2$ can be rationalized based on the following reactions:

$$TiN : \quad TiCl_4 + 4\,KNH_2 \rightarrow Ti(NH_2)_4 + 4\,KCl$$

$$3\,Ti(NH_2)_4 \rightarrow TiN + 8\,NH_3 + 2\,N_2$$

$$ZnSiN_2 : \quad [Zn\{Si(NMe_2)_2(NH^tBu)(NC^tBu)\}(\mu\text{-}C_5H_4N)]_2 \rightarrow$$
$$2\,ZnSiN_2 + 4\,NMe_2{}^tBu + 2\,C_5H_5N$$

Subsequent to synthesis, the TiN and $ZnSiN_2$ nanoparticles were purified by repeated centrifugation/redispersion in/from methanol (to remove KCl) or pyridine (to remove $NMe_2{}^tBu$). Finally, the nanoparticles can be easily redispersed in pyridine or toluene to obtain colloidally stable suspensions, or they were dried in vacuum to obtain po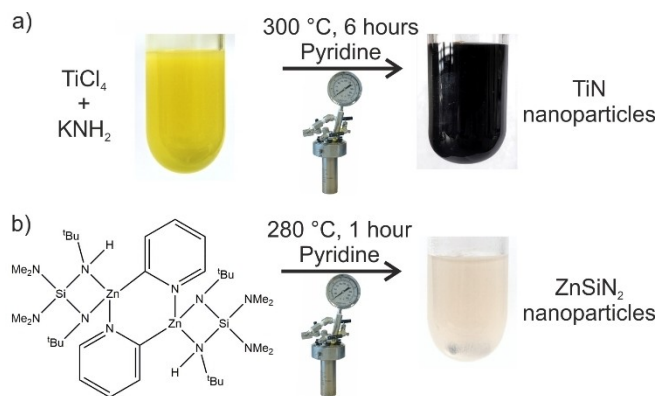wder samples. Powder samples of deep black TiN and colorless $ZnSiN_2$ were obtained with yields of 90–95% and can be redispersed in pyridine or toluene with 1–5 mg/mL.

Specific advantages of the novel pyridine-based approach relate to the absence of all oxygen sources (e.g. starting materials, surface functionalization, solvent) in the synthesis to strictly avoid oxide impurities. Even on a ppm-level, such oxide impurities could deteriorate the material properties and hamper the crystallization of the nitrides. Moreover, heating in pyridine to 280–300 °C turned out to be suitable to crystallize the metal nitrides instantaneously in the liquid phase. Finally, the moderately coordinating properties of pyridine and its weakly alkaline behavior allow controlling the particle nucleation and promote the ammonolysis at low temperature.[6,7]

2.2. Particle Size and Material Crystallinity

Particle size, size distribution and particle shape of the as-prepared TiN and $ZnSiN_2$ nanoparticles were determined by dynamic light scattering (DLS) and transmission electron microscopy (TEM). Thus, re-dispersed nanoparticles in pyridine exhibit mean diameters of 5.4 ± 0.4 nm for TiN and 5.2 ± 1.1 nm for $ZnSiN_2$ (Figure 2). Overview TEM images of both compounds show rather uniform nanoparticles with particle sizes clearly below 10 nm (Figure 3a,d). High-resolution transmission electron microscopy (HRTEM) images, furthermore, confirm particle sizes of about 4–6 nm for TiN and $ZnSiN_2$ (Figure 3b,e). This size is in agreement with the slightly larger hydrodynamic diameter obtained from DLS analysis.

HRTEM images of the TiN and $ZnSiN_2$ nanoparticles clearly show pronounced lattice fringes that indicate the crystallinity of the as-prepared nanoparticles (Figure 3b,e). The observed lattice distances of 2.1 Å (TiN) and 2.5 Å ($ZnSiN_2$) are well compatible with the bulk compounds (d_{200} of bulk-TiN: 2.13 Å; d_{002} of bulk-$ZnSiN_2$: 2.54 Å).[15d,16] Fourier transformations of the HRTEM images confirm the crystallinity of the as-prepared nanoparticles and are in accordance with the cubic lattice symmetry of NaCl-type TiN (space group *Fm-3m*) and the wurtzite-type $ZnSiN_2$ (space group *P6₃mc*) (Figure 3c,f).

Besides single nanoparticles on TEM images, the crystallinity of the as-prepared TiN and $ZnSiN_2$ nanoparticles was as well validated for powder samples by X-ray powder diffraction (XRD) for a statistically relevant number of nanoparticles (Figure 4).
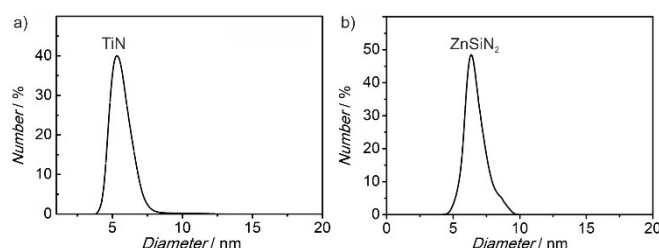

Figure 1. Schematic synthesis of TiN and $ZnSiN_2$ nanoparticles via a one-pot liquid-phase synthesis in pyridine.

Figure 2. Particle size and particle size distribution of the as-prepared TiN and $ZnSiN_2$ nanoparticles after re-dispersion in pyridine according to DLS analysis.

ChemistryOpen

Full Papers
doi.org/10.1002/open.202000315

Chemistry
Europe
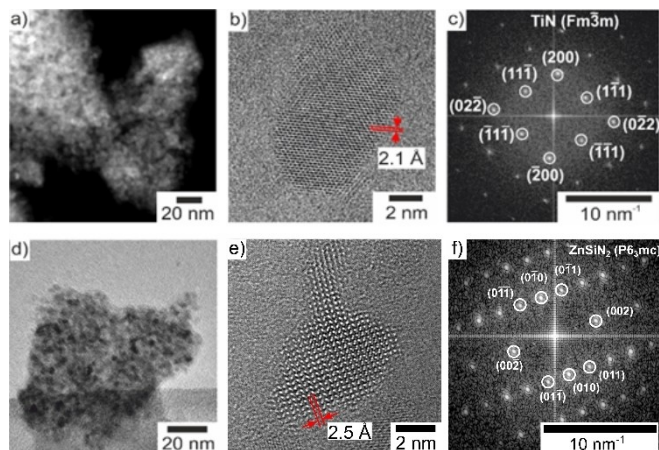European Chemical
Societies Publishing

Figure 3. Particle size and crystallinity of the as-prepared TiN and ZnSiN$_2$ nanoparticles: a) High-angle annular dark-field scanning transmission electron microscopy (HAADF-STEM) overview and b) HRTEM images of TiN; c) FT analysis of the HRTEM image in (b) along the [011] zone axis; d) TEM overview and e) HRTEM images of ZnSiN$_2$, f) FT analysis of the HRTEM image in (e) along the [100] zone axis.
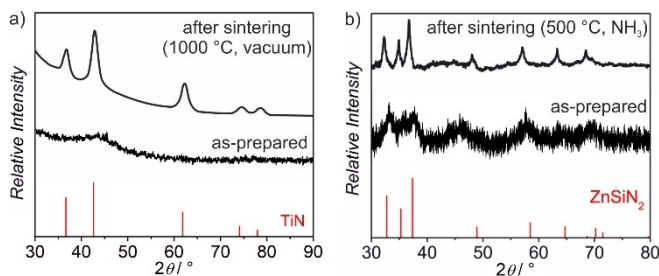

Figure 4. Crystallinity of TiN (a) and ZnSiN$_2$ (b) nanoparticles according to XRD after synthesis and after sintering (TiN at 800 °C in vacuum; ZnSiN$_2$ at 500 °C in NH$_3$ atmosphere) with references diffractograms (TiN: ICDD-No. 01-071-0299;[16] ZnSiN$_2$: CSD-No. 412711, powder diffractogram calculated from data of single-crystal structure analysis).[15d]

Although the as-prepared nanoparticles show only weak scattering intensities, the most intense Bragg reflections are clearly visible as broad, low intensity peaks. Broad peak width and low intensity, in fact, are to be expected in view of the small particle and crystallite sizes of a few nanometers. Subsequent to sintering at 800 °C (TiN) and 500 °C (ZnSiN$_2$), the Bragg peaks of TiN and ZnSiN$_2$ are clearly visible (Figure 4). Although the particle size was significantly increased subsequent to sintering, X-ray diffraction patterns nevertheless confirm the purity of the title compounds and the absence of impurity phases (especially of metal oxides), which would have been crystallized by sintering as well.

In sum, HRTEM and XRD prove the crystallinity of the as-prepared TiN and ZnSiN$_2$ nanoparticles. Taking the slow solid-state diffusion in nitrides into account, this high crystallinity is surprising in view of the low temperature of synthesis (280–300 °C). Typically, completion of the ammonolysis and crystallization of metal nitrides require significantly higher temperatures ($\geq$ 600 °C). Moreover, a liquid-phase synthesis of crystalline TiN and ZnSiN$_2$ nanoparticles with a diameter below 10 nm was not reported so far.

2.2.1. Phase Purity

Since the realization of high-purity metal nitride nanoparticles is a specific challenge, which is highly relevant in regard of the material properties, we have especially addressed the phase purity of the as-prepared TiN and ZnSnN$_2$ nanoparticles. In this regard, Fourier-transform spectroscopy (FT-IR), elemental analysis (EA), energy-dispersive X-ray spectroscopy (EDXS) and electron-energy loss spectroscopy (EELS) were performed.

FT-IR spectroscopy is an indicative tool to validate the completion of the ammonolysis and to evaluate the surface conditioning of the as-prepared nanoparticles (Figure 5). As expected, the characteristic vibrations of pyridine are observed, which can be ascribed to pyridine attached to the surface of the nanoparticles. The absence of N–H and O–H vibrations, moreover, indicates the completeness of the ammonolysis (i.e. absence of amides and imides) as well as the exclusion of any hydrolysis (i.e. absence of hydroxides) (Figure 5). All in all, FT-IR spectroscopy also confirms the purity of the TiN and ZnSiN$_2$ nanoparticles with only pyridine remaining as a surface capping.

EA (N/C/H analysis) points to significant amounts of nitrogen as well as minor amounts of carbon and hydrogen (Table 1). With the metals (Ti, Zn + Si) representing the remaining part, the composition is well in agreement with TiN and ZnSiN$_2$. This is specifically indicated by the ratio of atoms, which is close to the expected ratios of Ti:N = 1:1 and (Zn + Si):N = 1:1 (Table 1). It should be noted that the C:H ratios of 11:1 (TiN) and 12:1 (ZnSiN$_2$) relate to pyridine (C:H = 12:1), which again confirms the surface functionalization of the nanoparticles with pyridine. Due to the presence of pyridine, finally, the amount of the metal atoms is slightly smaller and the nitrogen content slightly larger than calculated (Table 1). More-
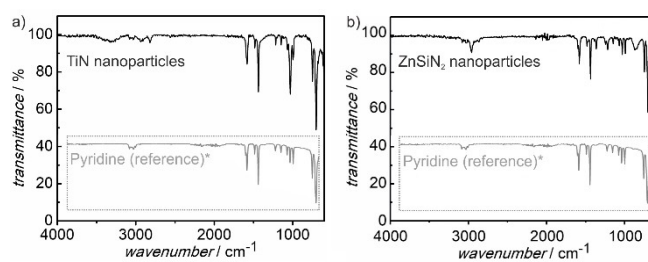

Figure 5. FT-IR spectra of TiN (a) and ZnSiN$_2$ (b) nanoparticles with spectrum of pure pyridine as a reference (transmission of reference spectrum with arbitrary units).

Table 1. Composition of TiN and ZnSiN$_2$ nanoparticles according to elemental analysis (C/H/N analysis).

Element	TiN/wt% (observed)	TiN/wt% (calculated)	ZnSiN$_2$/wt% (observed)	ZnSiN$_2$/wt% (calculated)
N	21.0	22.6	22.7	23.0
C	5.4	0	4.6	0
H	0.5	0	0.4	0
Remain	73.1 (Ti)	77.4 (Ti)	72.3 (Zn + Si)	76.9 (Zn + Si)
Ratio[a]	0.96 (Ti:N)	1 (Ti:N)	1.08 ($\frac{Zn+Si}{N}$)	1 ($\frac{Zn+Si}{N}$)

[a] Ratio calculated based on at-% of the elements.

© 2020 The Authors. Published by Wiley-VCH GmbH

ChemistryOpen

Full Papers
doi.org/10.1002/open.202000315

Chemistry Europe
European Chemical
Societies Publishing

over, EDXS indicates a Ti:N ratio of 0.9:1 and a Zn : Si:N ratio of 1.1:1.0:2 (scaled on nitrogen), which is well in agreement with the expected ratios of 1:1 and 1:1:2, respectively.

Finally, the purity of the as-prepared TiN nanoparticles was exemplarily examined by EELS. Due to the good energy resolution, EELS is a powerful tool to probe the presence of
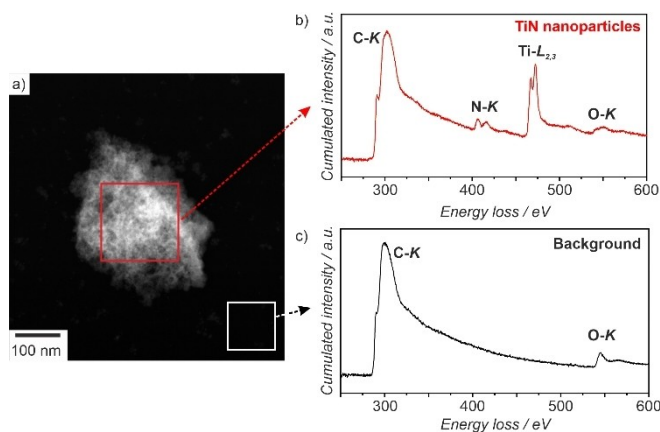

Figure 6. EEL spectra of agglomerated TiN nanoparticles: a) HAADF-STEM image; b) EEL spectrum acquired in red frame in (a); c) EEL reference spectrum acquired in white frame in (a) on the amorphous carbon support film.
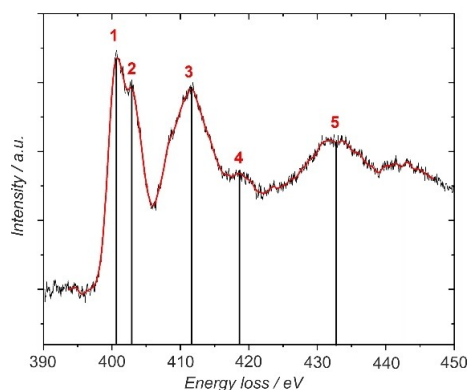

Figure 7. EELS spectrum of the N-K edge of the as-prepared TiN nano-particles with specific structural features indicated by red numbers (black line: experimental data, red line: smoothed curve).

crystalline titanium oxide phases. Specifically, the fine structure of the core loss ionization edges (ELNES: electron-loss near-edge structure) contains information related to unoccupied electronic states and the local atomic environment, which facilitates the distinction between amorphous and different crystalline phases. The EELS spectrum of agglomerated TiN nanoparticles show clearly separated C-K, N-K, Ti-$L_{2,3}$, and O-K ionization edges in the energy loss range between 280 and 575 eV (Figure 6a,b). The C-K and O-K edges are similarly observed in the EEL spectrum of the Lacey carbon film (Figure 6c). The pronounced O-K edge of the Lacey carbon film suggests that O in the spectrum of the TiN particles does not result from a crystalline titanium oxide phase but from an oxygen contamination of the carbon support film.

Energy position and shape of the N-K edge are in good agreement with literature data of bulk-TiN and indicate the crystallinity and purity of the as-prepared nanoparticles.[17] In particular, the ELNES of the N-K edge (Figure 7) can be assigned to electronic states of TiN using previous studies of cubic TiN.[17,18] Specifically, the double-peak structure at energy losses of 401/403 eV corresponds to the t_{2g} (401 eV) and e_g (403 eV) states of unoccupied N-$2p$ levels hybridized with Ti-$3d$ states (Figure 7: peaks 1 + 2,). The broad peak at 408–415 eV indicates unoccupied N-$2p$ states hybridized with Ti-$4s$ and Ti-$4p$ states (Figure 7: peak 3).[17] Peaks 4 and 5 are also present in the N-K edge measured by Kihn *et al.*.[17]

2.2.2. Material Properties

Based on the successful realization of crystalline TiN and $ZnSiN_2$ nanoparticles via the novel pyridine-based synthesis, we have exemplary addressed the optical properties of $ZnSiN_2$. First of all, the as-prepared $ZnSiN_2$ nanoparticles were evaluated by ultraviolet/visible (UV/Vis) spectroscopy (Figure 8a). Here, strong absorption is observed below 350 nm with certain tailing up to 550 nm. A Tauc plot indicates an indirect optical band gap of 3.2 eV (Figure 8b). This value is below values reported for bulk-$ZnSiN_2$ obtained via ammonothermal synthesis (3.6–3.7 eV),[15b,19] but well in agreement with calculated data (3.2 eV).[20] Additional low-intensity energy states are again observed within the band gap (so-called Urbach tailing)[21] and
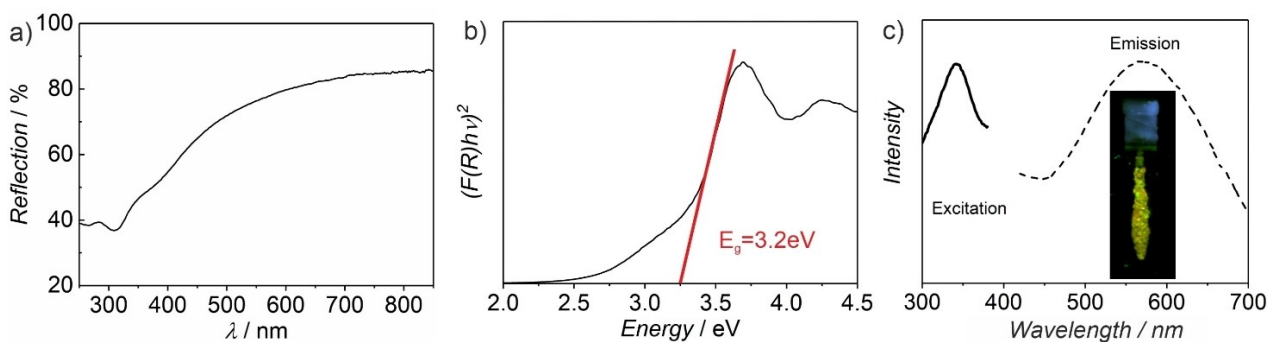

Figure 8. Optical properties of the as-prepared $ZnSiN_2$ nanoparticles: a) UV-Vis spectrum, b) Tauc plot to obtain the band gap; c) excitation and emission spectra with photo showing the yellowish emission of a powder sample at room temperature (excited at 366 nm).

ChemistryOpen

Full Papers
doi.org/10.1002/open.202000315

**Chemistry
Europe**
European Chemical
Societies Publishing

can be related most probably to surface states of the small-sized nanoparticles. Despite of these defect states, visible emission is already visible at room temperature. Thus, emission spectra indicate broad, yellowish emission in the 500-to-700 nm range with its maximum at 570 nm (Figure 8c). Excitation spectra, moreover, show valence-band-to-conduction-band absorption below 400 nm. Such visible emission of $ZnSiN_2$ nanoparticles is observed for the first time and even more remarkable when considering the small size of 4 nm of the nanoparticles. Upon band-gap excitation at 340 nm, the TiN nanoparticles exhibit a quantum yield of about 10% for the yellow emission. This is a typical value for semiconductor-type luminescence without establishing specific donor-acceptor levels. Since the feasibility of the pyridine-based synthesis has been now demonstrated in principle, additional measures such as selected doping and/or core-shell structures can promote a further significant increase of the emission intensity of the $ZnSiN_2$ nanoparticles.

3. Conclusions

Metal nitride nanoparticles not only require uniform size and low degree of agglomeration, but also high purity and high crystallinity to develop their potential of their material properties. Conventional methods, on the one hand, suffer from the low reactivity of N_2 (for nitridation reactions) or the high basicity of NH_3 (for ammonolysis reactions). Moreover, oxygen impurities, which can deteriorate the material properties even on a ppm level, can hardly be avoided if oxygen-containing components (e.g. starting materials, surface functionalization, solvents) are applied for synthesis. These limitations are here addressed with a novel pyridine-based synthesis and probed in regard of TiN and $ZnSiN_2$ nanoparticles as exemplary metal nitrides.

With this pyridine-based one-pot strategy, crystalline TiN and $ZnSiN_2$ nanoparticles can be instantaneously obtained from the liquid phase, resulting in colloidally stable suspensions of TiN (5.4±0.4 nm) and $ZnSiN_2$ (5.2±1.1 nm). Elemental analysis and electron energy loss spectroscopy confirm the purity of the compounds and specifically the absence of oxygen. The as-prepared $ZnSiN_2$ nanoparticles show yellowish emission (500–700 nm) even at room temperature. All-in-all, a liquid-phase synthesis of crystalline TiN and $ZnSiN_2$ nanoparticles with particle sizes <10 nm is here shown for the first time. In addition to the group 4 and 14 metal-nitride semiconductors TiN and $ZnSiN_2$ as examples, the pyridine-based synthesis route is of general relevance for the synthesis of crystalline, high-purity metal nitride nanoparticles and their material properties.

Experimental Section

General

All experiments and sample handling were performed under inert gas (argon) using standard Schlenk techniques and glove boxes. This explicitly also includes all centrifugation and purification procedures. Specifically important is the preparation of the metal nitride nanoparticles for TEM analysis and the transfer into the electron microscope, which require handling in glove boxes and use of suitable transfer modules.

Materials

Pyridine (ABCR, 99%) was refluxed for three days and freshly distilled over CaH_2. Methanol (Sigma-Aldrich, 99.5%) was refluxed over Mg for three days. KNH_2 was synthesized by reacting potassium (Riedel-de-Haën, 99%) in liquid ammonia (Air Liquide, 99.98%) at $-50\,°C$ using Fe_2O_3 as catalyst, followed by filtering and drying in vacuum. Titanium(IV)chloride (Sigma-Aldrich, 99.9%) was used as purchased. $[Zn\{Si(NMe_2)_2(NHCMe_3)(NCMe_3)\}(\mu\text{-}NC_5H_4)]_2$ was prepared as reported by Jansen et al. (SI).[15d]

Synthesis of TiN Nanoparticles

0.05 ml of $TiCl_4$ were added to 20 ml of pyridine in an titanium autoclave (Parr Instruments, USA), resulting in a yellow suspension of $TiCl_4(Py)_2$. Subsequently to the addition of 95 mg of KNH_2, the autoclave was deposited in a pre-heated heating jacket (300 °C). This temperature was kept for 6 hours. Thereafter, heating was stopped and the autoclave was allowed to cool to room temperature. As a result, a deep black suspension was obtained. The TiN nanoparticles were purified by repeated centrifugation/redispersion in/from methanol (25.000 U/min, 55.201 g). They can be easily redispersed in pyridine or dried in vacuum to obtain powder samples.

Synthesis of $ZnSiN_2$ Nanoparticles

About 100 mg of $[Zn\{Si(NMe_2)_2(NHCMe_3)(NCMe_3)\}(\mu\text{-}NC_5H_4)]_2$ were dissolved in 10 ml pyridine and transferred into an titanium autoclave (Parr Instruments, USA). The autoclave was deposited in a pre-heated heating-jacket (280 °C). This temperature was kept for one hour. Thereafter, heating was stopped and the autoclave was allowed to cool to room temperature. As a result, a colorless suspension was obtained. The $ZnSiN_2$ nanoparticles were washed by repeated re-dispersion/centrifugation (25.000 U/min, 55.201 g) in/from pyridine. Thereafter, the $ZnSiN_2$ nanoparticles can easily be re-dispersed in pyridine or dried in vacuum in order to obtained powder samples. Optional sintering was performed at 500 °C in NH_3 atmosphere.

Conflict of Interest

The authors declare no conflict of interest.

ChemistryOpen

Full Papers
doi.org/10.1002/open.202000315

**Chemistry
Europe**
European Chemical
Societies Publishing

[1] *Reviews:* a) R. E. Karaballi, Y. E. Monfared, M. Dasog, *Chem. Eur. J.* **2020**, *26*, 8499–8505; b) L. Xu, S. Li, Y. Zhang, Y. Zhai, *Nanoscale* **2012**, *4*, 4900–4915; c) C. Giordano, M. Antonietti, *Nano Today* **2011**, *6*, 366–380.

[2] a) O. Majoulet, C. Salameh, M. E. Schuster, U. B. Demirci, Y. Sugahara, S. Bernard, P. Miele, *Chem. Mater.* **2013**, *25*, 3957–3970; b) J. Choi, E. G. Gillan, *Inorg. Chem.* **2005**, *44*, 7385–7393; c) W. Yang, Z. Xie, H. Miao, L. Zhang, H. Ji, L. An, *J. Am. Ceram. Soc.* **2005**, *88*, 466–469; d) A. Manz, A. Birkner, M. Kolbe, R. A. Fischer, *Adv. Mater.* **2000**, *12*, 569–573.

[3] *Review:* T. M. M. Richter, R. Niewa, *Inorganics* **2014**, *2*, 29–78.

[4] C. G. van de Walle, J. Neugebauer, *J. Appl. Phys.* **2004**, *95*, 3851–3879.

[5] *Review:* H. Goesmann, C. Feldmann, *Angew. Chem. Int. Ed.* **2010**, *49*, 1362–1395; *Angew. Chem.* **2010**, *122*, 1402–1437.

[6] a) A. Egeberg, T. P. Seifert, P. W. Roesky, D. Gerthsen, C. Feldmann, *ACS Omega* **2019**, *4*, 7096–7102; b) A. Egeberg, T. Block, O. Janka, O. Wenzel, D. Gerthsen, R. Pöttgen, C. Feldmann, *Small* **2019**, *15*, 1902321(1–9).

[7] A. Egeberg, L. Warmuth, S. Riegsinger, D. Gerthsen, C. Feldmann, *Chem. Commun.* **2018**, *54*, 9957–9960.

[8] a) S. Ishii, R. P. Sugavaneshwar, T. Nagao, *J. Phys. Chem. C* **2016**, *120*, 2343–2348; b) U. Guler, V. M. Shalaev, A. Boltasseva, *Mater. Today* **2015**, *18*, 227–237; c) B. Avasarala, T. Murray, W. Li, P. Haldar, *J. Mater. Chem.* **2009**, *19*, 1803–1805; d) A. D. Martinez, A. N. Fioretti, E. S. Toberer, A. C. Tamboli, *J. Mater. Chem. A* **2017**, *5*, 11418–11435; e) A. Punya, W. R. L. Lambrecht, M. van Schilfgaarde, *Phys. Rev. B* **2011**, *84*, 165204/1–10.

[9] a) E. B. Clatworthy, S. Yick, A. T. Murdock, M. C. Allison, A. Bendavid, A. F. Masters, T. Maschmeyer, *J. Phys. Chem. C* **2019**, *123*, 3740–3749; b) X. Peng, A. M. Qasim, W. Jin, L. Wang, L. Hu, Y. Miao, W. Li, Y. Li, Z. Liu, K. Huo, *Nano Energy* **2018**, *53*, 66–73.

[10] a) Z. Xiu, D. Kim, M. H. Alfaruqi, J. Gim, J. Song, S. Kim, P. T. Duong, J. P. Baboo, V. Mathew, J. Kim, *J. Mater. Chem. A* **2016**, *4*, 4706–4710; b) F. Li, R. Ohnishi, Y. Yamada, J. Kubota, Y. Domen, A. Yamada, H. Zhou, *Chem. Commun.* **2013**, *49*, 1175–1177.

[11] a) H. Sugimoto, Y. Ikuno, M. Fujii, *ACS Appl. Nano Mater.* **2019**, *2*, 6769–6773; b) U. Guler, J. C. Ndukaife, G. V. Naik, A. G. A. Nnanna, A. V. Kildishev, V. M. Shalaev, A. Boltasseva, *Nano Lett.* **2013**, *13*, 6078–6083.

[12] a) A. W. Jackson, O. Shebanova, A. L. Hector, P. F. McMillan, *J. Solid State Chem.* **2006**, *179*, 1383–1393; b) K. Schlichte, G. Chaplais, M. Khanna, S.

Kaskel, *J. Mater. Chem.* **2003**, *13*, 1496–1499; c) K. Schlichte, T. Kratzke, S. Kaskel, *J. Mol. Catal. A* **2004**, *1*, 291–298.

[13] a) I. S. Kim, P. N. Kumta, *J. Mater. Chem.* **2003**, *13*, 2028–2035; b) J. Hu, Q. Lu, K. Tang, S. Yu, Y. Qian, G. Zhou, X. Liu, *J. Am. Ceram. Soc.* **2000**, *83*, 430–432.

[14] a) A. A. Popov, G. Tselikov, N. Dumas, C. Berard, K. Metwally, N. Jones, A. Al-Kattan, B. Larrat, D. Braguer, S. Mensah, *Sci. Rep.* **2019**, *9*, 1–11; b) S. Sakaki, K. Saitow, M. Sakamoto, H. Wada, Z. Swiatkowska-Warkocka, Y. Ishikawa, N. Koshizaki, *Appl. Phys. Express* **2018**, *11*, 035001/1–4.

[15] a) N. L. Adamski, D. Wickramaratne, C. G. Van de Walle, *J. Mater. Chem. C* **2020**, *8*, 7890–7898; b) J. Häusler, S. Schimmel, P. Wellmann, W. Schnick, *Chem. Eur. J.* **2017**, *23*, 12275–12282; c) B. P. Cook, H. O. Everitt, I. Avrutsky, A. Osinsky, A. Cai, J. F. Muth, *Appl. Phys. Lett.* **2005**, *86*, 121906; d) J. Engering, M. Jansen, *Z. Anorg. Allg. Chem.* **2003**, *629*, 109–115; e) A. Mintairov, J. Merz, *Appl. Phys. Lett.* **2000**, *76*, 2517–2519; f) T. Endo, Y. Sato, H. Takizawa, M. Shimada, *J. Mater. Sci. Lett.* **1992**, *11*, 424–426.

[16] A. N. Christensen, *Acta Chem. Scand.* **1978**, *32*, 89.

[17] Y. Kihn, C. Mirguet, L. Calmels, *J. Electron Spectrosc. Relat. Phenom.* **2005**, *143*, 117–127.

[18] L. Soriano, M. Abbate, H. Pen, M. Czyzyk, J. C. Fuggle, *J. Electron Spectrosc. Relat. Phenom.* **1993**, *62*, 197–206.

[19] T. Endo, Y. Sato, H. Takizawa, M. Shimada, *J. Mater. Sci. Lett.* **1992**, *11*, 424–426.

[20] a) Y. Bai, G. Luo, L. Meng, Q. Zhang, N. Xu, H. Zhang, X. Wu, F. Konga, B. Wang, *Phys. Chem. Chem. Phys.* **2018**, *20*, 14619–14626; b) A. Punya, W. R. L. Lambrecht, *Phys. Rev. B* **2011**, *84*, 165204; c) J. Rufinus, *J. Appl. Phys.* **2009**, *105*, 07 C509.

[21] S. Zaynobidinov, R. G. Ikramov, R. M. Jalalov, *J. Appl. Spectrosc.* **2011**, *78*, 223–227.